Direct observation of phase coherence in 3-k magnetic configurations

Elizabeth Blackburn, Nicholas Bernhoeft, Garry James Mcintyre, Stuart B. Wilkins, Pascal Boulet, Jacques Ollivier, Andrew Podlesnyak, Fanni Juranyi, Pavel Javorský, Gh Lander, et al.

Direct observation of phase coherence in 3-k magnetic configurations

Journal:	*Philosophical Magazine & Philosophical Magazine Letters*
Manuscript ID:	TPHM-05-Jan-0021.R1
Journal Selection:	Philosophical Magazine
Date Submitted by the Author:	06-Jun-2005
Complete List of Authors:	Blackburn, Elizabeth; Institute for Transuranium Elements, Actinide Research Unit; Institut Laue-Langevin Bernhoeft, Nicholas; CEA, DRFMC McIntyre, Garry; Institut Laue-Langevin Wilkins, Stuart B.; Institute for Transuranium Elements, Actinide Research Unit; European Synchrotron Radiation Facility Boulet, Pascal; Institute for Transuranium Elements, Actinide Research Unit Ollivier, Jacques; Institut Laue-Langevin Podlesnyak, Andrew; ETHZ & PSI, Laboratory for Neutron Scattering Juranyi, Fanni; ETHZ & PSI, Laboratory for Neutron Scattering Javorský, Pavel; Institute for Transuranium Elements, Actinide Research Unit Lander, GH; Institute for Transuranium Elements, Actinide Research Unit Mattenberger, Kurt; ETH Zurich, Laboratorium für Festkorperphysik Vogt, Oscar; ETH Zurich, Laboratorium für Festkörperphysik
Keywords:	neutron scattering, magnetic structure
Keywords (user supplied):	multiple order parameters
Note: The following files were submitted by the author for peer review, but cannot be converted to PDF. You must view these files (e.g. movies) online.	

Blackburn_Manuscript.zip

Direct observation of phase coherence in 3-k magnetic configurations

E. BLACKBURN[†,‡], N. BERNHOEFT[*¶], G. J. McINTYRE[‡], S. B. WILKINS[†,§], P. BOULET[†], J. OLLIVIER[‡], A. PODLESNYAK[‖], F. JURANYI[‖], P. JAVORSKY[†], G. H. LANDER[†], K. MATTENBERGER[♯] and O. VOGT[♯]

† European Commission, JRC, Institute for Transuranium Elements, Postfach 2340, Karlsruhe D-76125, Germany.
‡ Institut Laue-Langevin, BP 156, F-38042 Grenoble, France.
¶ CEA, DRFMC, F-38054 Grenoble, France.
§ European Synchrotron Radiation Facility, BP 220, F-38043 Grenoble, France.
‖ Laboratory for Neutron Scattering, ETH Zürich and PSI, CH-5232 Villigen PSI, Switzerland.
♯ Laboratorium für Festkörperphysik, ETH Zürich, CH-8093 Zurich, Switzerland.

Abstract

We report the observation by neutron diffraction of phase coherent Bragg reflections in a multi-**k** magnetic configuration with a spatial periodicity outside the conventional scattering cross-section. The peaks, which exist in the 3-**k** state of $UAs_{0.8}Se_{0.2}$, display long-range order with a wavevector dependence characteristic of a magnetic interaction. The results confirm the long-range order and temperature dependence reported in an earlier study of similar peaks in this material using x-ray resonant scattering by (a) the non-trivial extension to the technique of neutron diffraction, and (b) the observation of similar 3-**k** phase-coherent reflections in other samples by x-ray resonant scattering. The importance of the neutron diffraction results lies primarily in the fact that magnetic neutron diffraction is well established as a weak probe operating on thermodynamic time scales. This alleviates concern that the rapid (10^{-15} - 10^{-14} s), strong interaction, characteristic of the resonant x-ray technique, is imaging a transient or non-equilibrium configuration. Likewise, the extension of the x-ray resonant scattering results to other samples establishes the generality of this effect.

The enigma of how to understand the observed diffraction, which appears to lie strictly outside both the conventional neutron and x-ray scattering cross sections, remains.

Keywords: neutron scattering; non-collinear magnetic structures; multiple order parameters

1 Introduction

Neutron scattering is a powerful probe of space-time correlations in condensed matter. In particular, since the neutron carries a magnetic moment, it is sensitive to the magnetic field distribution in the sample. This technique has long been exploited in studies of magnetic materials. The scattering cross-section can be directly related to the microscopic current-density auto-correlation function. A physically appealing interpretation of experimental data may be given by introducing the magnetisation as an order parameter [1-3].

Ferromagnets and coplanar magnetic structures (e.g. Néel antiferromagnets and helical magnetic structures) are described by an on-site term $\mathcal{M}_{\mathbf{k}_\alpha} =$

$\mathbf{M}_{\mathbf{k}_\alpha}\exp(i\theta_{\mathbf{k}_\alpha})$, where $\mathbf{M}_{\mathbf{k}_\alpha}$ is the polarisation vector and $\theta_{\mathbf{k}_\alpha} = \mathbf{k}_\alpha.\mathbf{r}_i + \theta_\alpha$ is the relative phase at the i^{th} position. Such magnetic configurations are specified by one polarisation vector and one propagation vector, $\mathbf{k}_\alpha$, and are nominated single-$\mathbf{k}$ magnetic structures.

The discovery by Kouvel and Kasper [4] of neutron diffraction patterns from Fe-Mn alloys that cannot be interpreted within this paradigm led to the proposal of multi-$\mathbf{k}$ configurations as a natural expansion of the single-$\mathbf{k}$ case. These intricate, non-collinear magnetic structures may be described by the simultaneous presence of more than one polarisation and associated propagation vector at a given site. For example, a configuration is deemed 2-$\mathbf{k}$ when, for a given reciprocal lattice vector τ, a single domain yields magnetic Bragg peaks corresponding with two (orthogonal) wavevectors [5]. In this scheme, a 2-$\mathbf{k}$ configuration is defined by two (orthogonal) simultaneous on-site terms, $\mathcal{M}_{\mathbf{k}_\alpha} = \mathbf{M}_{\mathbf{k}_\alpha}\exp(i\theta_{\mathbf{k}_\alpha})$ and $\mathcal{M}_{\mathbf{k}_\beta} = \mathbf{M}_{\mathbf{k}_\beta}\exp(i\theta_{\mathbf{k}_\beta})$, and therefore two independent order parameters. In practice, the existence of domains often makes it impossible to distinguish neutron diffraction peaks generated by a polydomain single-$\mathbf{k}$ structure from those generated by a multi-$\mathbf{k}$ configuration. Whilst aid in resolving this problem is available through the application of magnetic fields or uniaxial stress to perturb the domain population, neutron diffraction appears to be limited as a diagnostic tool. Such problems are compounded for 3-$\mathbf{k}$ magnetic structures.

Nevertheless, careful neutron and x-ray diffraction studies of $UAs_{0.8}Se_{0.2}$ (NaCl structure, with the Se ions randomly substituted on As sites) in both zero and applied magnetic field [6, 7] have revealed three, distinct, multi-$\mathbf{k}$ magnetic structures. Figure 1 gives the magnetic and crystallographic phase lines as a function of temperature. The low-temperature commensurate 2-$\mathbf{k}$ (tetragonal crystal structure) phase undergoes a transition at T^* ($\sim$ 50 K) to a 3-$\mathbf{k}$ magnetic configuration having a cubic unit cell. In both phases, the magnetic propagation vector is $\langle 00k\rangle = \langle 0\ 0\ 1/2\rangle$ in reciprocal lattice units (rlu). At T_o = 119 K the 3-$\mathbf{k}$ configuration becomes incommensurate prior to the transition to the paramagnetic state above T_N = 124 K.

[Insert Figure 1 here]

The single-$\mathbf{k}$ reflections in this material are found by neutron diffraction at wavevectors of the form $\mathbf{k_1} = \tau + \langle 00k\rangle$ where τ, the reciprocal lattice vector, is not parallel to $\langle 00k\rangle$. They form the basis of the 2- and 3-$\mathbf{k}$ descriptions of the magnetic configurations by Kuznietz *et al.* [6]. However, direct confirmation of the long-range phase coherence between the independent order parameters, which would be available through Bragg peaks of the form $\mathbf{k_2} = \tau + \langle 0kk\rangle$ and $\mathbf{k_3} = \tau + \langle kkk\rangle$ in 2- and 3-$\mathbf{k}$ states respectively, appears to lie outside the conventional formulation of the neutron diffraction cross section. To see this, consider the structure factor $\mathbf{F}(\mathbf{Q}) = \sum_i \mathbf{m}_i\exp(i\mathbf{Q}.\mathbf{d}_i)$ where $\mathbf{Q}$ is the scattering vector, and $\mathbf{m}_i$ is the scattering amplitude of the magnetic moment located at position $\mathbf{d}_i$ in real space. In a multi-$\mathbf{k}$ structure this scattering amplitude is the sum of the on-site terms $\mathcal{M}_\alpha$. In the triple-$\mathbf{k}$ case,

$$\mathbf{m}_i = \mathbf{M}_{\mathbf{k}_x}\exp(i\mathbf{k}_x.\mathbf{d}_i + i\theta_x) + \mathbf{M}_{\mathbf{k}_y}\exp(i\mathbf{k}_y.\mathbf{d}_i + i\theta_y) + \mathbf{M}_{\mathbf{k}_z}\exp(i\mathbf{k}_z.\mathbf{d}_i + i\theta_z)$$

where $\mathbf{k}_x = [1/2\ 0\ 0]$, $\mathbf{k}_y = [0\ 1/2\ 0]$, $\mathbf{k}_z = [0\ 0\ 1/2]$ and $\theta_x = \theta_y = \theta_z = \pi/4$. These three independent terms will, in turn, be non-zero at the appropriate $\mathbf{k_1}$ vector, $\mathbf{Q} = \mathbf{k_1} = \tau + \langle 00k\rangle$. However, all terms are necessarily zero at both $\mathbf{k_2} = \tau + \langle 0kk\rangle$ and $\mathbf{k_3} = \tau + \langle kkk\rangle$ positions.

Recently it was perceived that direct evidence for 2-**k** phase coherence may be forthcoming by the imaging of $\mathbf{k_2}$ reflections using x-ray scattering techniques at the uranium electric dipole (E1) resonance [8]. However, at this resonance, the calculated 3-**k** cross-section is zero, and so diffraction evidence for the 3-**k** phase remains apparently out of reach. Notwithstanding this, using x-ray resonant scattering techniques, experimentalists found evidence for long-range order in the form of $\mathbf{k_3}$ diffraction peaks in the commensurate 3-**k** phase of $UAs_{0.8}Se_{0.2}$ [9, 10]. These reflections, which have an intensity of $\sim 10^{-4}$ of the $\mathbf{k_1}$ peaks at a given temperature, have been shown not to originate from multiple scattering or minority phases by their incident photon energy, azimuth, scattering wavevector and temperature dependent behaviour.

The aim of the present work is to establish the generality of these long-range ordered $\mathbf{k_3}$ peaks using both different samples and neutron diffraction in addition to x-ray resonant diffraction, and to establish a lower bound on the phase de-coherence time.

2 X-ray resonant scattering

X-ray resonant scattering from both the 3-**k** phase of $USb_{0.85}Te_{0.15}$ and a second sample of $UAs_{0.8}Se_{0.2}$ (detailed information on samples is given in Appendix A) have established the sample independence of the $\mathbf{k_3}$ peaks as measured on the ID20 beamline at the European Synchrotron Radiation Facility (ESRF), Grenoble, France. Likewise, any qualms based on the notion that the $\mathbf{k_3}$ peaks were an artifact arising from mixed $\mathbf{k_1}$-$\mathbf{k_2}$ processes in $UAs_{0.8}Se_{0.2}$ have been put to rest by the observations in $USb_{0.85}Te_{0.15}$, which has no 2-**k** state. In this context, since the phases of the $\mathbf{k_1}$ and $\mathbf{k_2}$ amplitudes are imaginary and real (as in Thompson scattering) respectively, in principle no static cross-term is possible. Figure 2 gives the azimuth dependence of the integrated intensities of the $\mathbf{k_3}$ (-1/2 -1/2 5/2) reflection from $USb_{0.85}Te_{0.15}$ together with the calculated azimuth dependence in the 3-**k** phase coherent state (solid line). The calculation is based on the $F^{(1)}$ term of the E1 x-ray cross section, as given in the appendix to Ref. [8]. Central to the calculation is the definition of a symmetry-breaking vector (effective dipole moment) parallel to the appropriate $\langle kkk \rangle$ vector needed to generate the given reflection. This yields an azimuth dependence on τ in agreement with observations in both Figure 2 and Refs. [8-10]. From this, it is inferred that the relative phasing between the three primary order parameters is a key characteristic of the $\mathbf{k_3}$ peaks. Furthermore, a similar symmetry-breaking vector appears in the interpretation of the neutron scattering data, as discussed below.

[Insert Figure 2 about here]

Since the resonant process is a strong, second-order probe of the electronic state and acts on a time scale $\sim 10^{-14}$s, which is close to the typical electronic hopping frequency, the $\mathbf{k_3}$ peaks may only be present on a quantum mechanical time scale and so may be a manifestation of electronic correlations of little relevance to the slow, low-energy dynamics that characterise the thermal state. The magnetic neutron interaction, which couples to first order in the vector potential and acts as a weak probe, has the advantage of yielding information on the two-site relative phase correlation function on thermodynamic time scales.

3 Neutron diffraction

Neutron diffraction studies were carried out on the four-circle diffractometer D10 at the Institut Laue-Langevin (ILL), Grenoble, France. To maximise the signal-to-noise ratio, the diffractometer was operated in triple-axis mode using a pyrolytic graphite (002) analyser crystal (estimated acceptance of ± 0.5 meV at full width half maximum) and a He^3 detector with maximal incident flux ($5 \cdot 10^6$ neutrons $cm^{-2}s^{-1}$) at the calibrated wavelength $\lambda = 2.3622(3)$ Å. In order to suppress $\lambda/2$ contamination, a pyrolytic graphite filter was placed in the path of the incident beam.

The sample of $UAs_{0.8}Se_{0.2}$ was the same as that used in Refs. [8-10]. The crystal was indexed at room temperature using the 66 accessible nuclear Bragg reflections, and checked at lower temperatures, giving a lattice parameter of 5.7694(11) Å at 65 K, with the error in λ included.

Bragg reflections indexed at $\mathbf{k_1} = \langle 1\ 1\ 1/2 \rangle$ confirm the presence of the single-**k** order parameters for $T < T_o$. The temperature dependence of three such $\mathbf{k_1}$ reflections is given in Figure 3, showing the long-range phase coherence of the orthogonal order parameters in the 3-**k** state ($T^* \leq T \leq T_o$), together with approximately equal domain populations below T^* in the 2-**k** state. This is consistent with the behaviour noted by Kuznietz *et al.* [6].

[Insert Figure 3 about here]

The three frames in Figure 4 show measurements at the (3/2 -1/2 -1/2) $\mathbf{k_3}$ position for $T < T^*, T^* < T < T_N$ and $T > T_N$ respectively. The peak is only present between T^* and T_N, i.e. in the 3-**k** phase. The intensity of this peak is approximately 10^{-3} of the strongest single-**k** magnetic reflections. For the 3-**k** description of the magnetic structure given by Kuznietz *et al.* [6], the geometric structure factor is zero at this position. The sharp wavevector response, indicative of long-range order, appears to eliminate parasitic phases as the origin, in agreement with the results obtained by x-ray diffraction [9, 10]. Further $\mathbf{k_3}$ reflections were measured. They exhibit a general decrease in integrated intensity with increasing scattering vector (measured out to 3.6 $Å^{-1}$), consistent with a magnetic origin for these reflections.

[Insert Figure 4 about here]

The temperature dependence of the (3/2 -1/2 -1/2) $\mathbf{k_3}$ peak is given in Figure 5, together with the $\mathbf{k_1}$ data and overlaid on equivalent x-ray data [9]. Although the neutron diffraction data are relatively poorly defined and few in number, they are consistent with x-ray data from the same sample. This, together with the long-range order and effective dipolar nature of the appropriate order parameter, suggests that the x-ray (near surface) and neutron (bulk) probes are imaging the same object.

[Insert Figure 5 about here]

Whilst $\mathbf{k_3}$ peaks are observed at positions where τ is not parallel to $\langle kkk \rangle$, they are (apparently systematically) absent at $\mathbf{k_3}$ positions such as (1/2 -1/2 -1/2) and (3/2 -3/2 -3/2). On account of the electromagnetic nature of the interaction [2], this implies that the effective magnetic moment lies parallel to the scattering vector, in this case [1 -1 -1]. Similarly, $\mathbf{k_1}$ peaks where τ is parallel to the ordering wavevector $\langle 00k \rangle$ are also absent. The inference from these two observations is that: (i) in common with the results obtained on the azimuth dependence of x-ray resonant scattering, the effective scattering object for the $\mathbf{k_3}$ peak may be parameterised by a moment which lies along the $\langle 111 \rangle$

directions, and (ii) for the $\mathbf{k_1}$ peak, the polarisation vector is parallel to the $\langle 001 \rangle$ directions. Whilst these two deductions can be reconciled at the classical level as a vector sum of 'components', this construction is unable to give a finite geometric structure factor at the $\mathbf{k_3}$ positions and, furthermore, any such linear combination of independent angular momenta appears to lack a sound microscopic basis.

Whereas the smooth and calculable azimuth response, as given in Figure 2, eliminates multiple scattering as a source of the $\mathbf{k_3}$ peaks in x-ray resonant scattering, the low intensities make azimuth scans by neutron diffraction more difficult. Nonetheless, a limited number of such scans have been performed on a selected $\mathbf{k_3}$ reflection and reveal no evidence for multiple scattering. Additionally, to generate a $\mathbf{k_3}$ peak by a multiple scattering process would require three $\mathbf{k_1}$ reflections. In this context, estimates of the expected magnitude of multiple scattering reflections are helpful.

The (1 1 1/2) $\mathbf{k_1}$ peak has 8.5% of the integrated intensity of the (002) nuclear reflection at 60 K. A multiple scattering signal was observed at positions of the $\mathbf{k_2}$ type, as confirmed by a Renninger scan. This had an intensity similar to that of the $\mathbf{k_3}$ peak. It involves a double scattering event, and this gives a reflectivity of $\sim 1\%$ for the (002). The implied multiple scattering event for a $\mathbf{k_3}$ reflection would therefore have a reflectivity of $6 \cdot 10^{-8}$ with respect to the (002) nuclear peak, leading to 10^{-2} counts on the scale shown in Figure 4. To obtain the observed signal via multiple scattering the reflectivity of the (002) would have to be ~ 25 %.

4 Neutron diffraction with time-of-flight analysis

Whilst the D10 data confirms the existence and long-range order of the $\mathbf{k_3}$ response, the phase coherence time window ($\sim 4 \cdot 10^{-12}$s) remains relatively coarse, being on the same scale as typical thermal excitations at these temperatures. When looking at low-level signals in $UAs_{0.8}Se_{0.2}$ a longer integration time may be important since inelastic neutron scattering on pure UAs shows a pronounced response, broad in wavevector and energy transfer, at temperatures below T_N [11]. To assess the degree of long-time order present in the correlations leading to the $\mathbf{k_3}$ response, the basis set of $\mathbf{k_1}$ diffraction peaks has been investigated by high resolution time-of-flight spectroscopy on a polycrystalline sample (details in Appendix). Attaining the necessary high resolution limits the count rate, rendering the $\mathbf{k_3}$ peaks unobservable.

Time-of-flight experiments have been carried out using the IN5 and FOCUS spectrometers, at the ILL and the Paul Scherrer Institute (PSI), Villigen, Switzerland, respectively. The spectrometers were operated at incident wavelengths (4.85, 5.13 and 5.30 Å) close to twice that used on D10, giving an elastic energy resolution better than 0.1 meV. The two-site de-coherence time can then be determined from the integrated elastic response on scales up to $\sim 4 \cdot 10^{-11}$s. The large solid angle detector banks enable a survey of the Brillouin zone for $0.25 \leq Q \leq 2.3$ Å^{-1}.

At the scattering angle corresponding with $\langle 1\ 1\ 1/2 \rangle$ magnetic reflections, the temperature dependences of the integrated elastic peak intensity, over an

energy transfer range $-0.15 \leq \Delta E \leq 0.15$ meV, and energy width are shown in panels (a) and (b) of Figure 6 respectively. In parallel with Figure 3 (single crystal data), they clearly show the transition from paramagnetism to magnetic order. The energy linewidth of the peak, panel (b), tracks the transition in the manner expected for a developing order parameter. In the paramagnetic phase, slow fluctuations with low amplitude generate a weak broadening of the elastic linewidth. In the immediate neighbourhood of T_N, the rapidly increasing fluctuation amplitude leads to a step-like increase in the measured width, followed by a sharp fall in the ordered phase. The reduced energy linewidth below T_N, despite the increasing integrated intensity, confirms the narrowing of the intrinsic linewidth and the long-time order of the independent single-$\mathbf{k}$ order parameters on time scales $\sim 10^{-11}$s. This result, which establishes the existence on thermodynamic space-time scales of the order parameter basis set for both the 2- and 3-$\mathbf{k}$ magnetic configurations, is important in view of the apparent conflicting requirements of angular momentum quantization with orthogonal magnetic moments in the given 3-$\mathbf{k}$ structure [6].

In addition to this response at the $\mathbf{k_1}$ positions, a significant increase in the intensity with *decreasing* temperature is seen across the full range of reciprocal space covered for all $T \leq T_N$ (Figure 6c). At all temperatures measured this integrated elastic scattering has a similar energy width (Figure 6d) to that observed at the $\mathbf{k_1}$ position in the paramagnetic phase above T_N (Figure 6b). Its broad extent in momentum transfer indicates that the response is generated by local, long-time correlations, the amplitude of which mimics the temperature dependence of the $\mathbf{k_1}$ antiferromagnetic Bragg peaks. The fact that it stays on a similar dynamic scale in both the paramagnetic and ordered phases suggests that it may be associated with a set of spatially incoherent minimal scattering units, as found in $YbSnPd_2$ [12].

[Insert Figure 6 about here]

5 Summary

The present results, which show x-ray and neutron diffraction peaks at $\mathbf{k_3}$ positions lying outside the respective scattering cross sections, confirm the sample independence of earlier x-ray resonant scattering results [9, 10] and yield complementary information on the nature and space-time coherence scales of the response. Potential worries associated with the fast and strongly perturbing character of the x-ray resonant scattering technique, multiple scattering and extinction effects in single crystal samples are allayed. Multiple scattering concerns in the neutron diffraction experiments are laid to rest by the (limited) azimuth scans together with estimates based on the reflectivity of the $\mathbf{k_1}$ peaks. Both single crystal data, integrated over $-1 \leq \Delta E \leq 1$ meV, and polycrystalline data, integrated over $-0.15 \leq \Delta E \leq 0.15$ meV, confirm that the observed $\mathbf{k_3}$ peaks are several orders of magnitude too strong to be associated with any (improbable) triple scattering event. The D10 diffraction data, taken in triple-axis mode (correlation time $\tau_c \sim 10^{-12}$s) on the same single crystal as used in the x-ray resonant diffraction experiments ($\tau_c \sim 10^{-14}$s), show that the $\mathbf{k_3}$ peaks exist on the temporal time scale of the thermodynamic state. Furthermore, the long-range, long-time order observed with respect to the three primary order parameters through $\mathbf{k_1}$ peaks on both D10 and the time-of-flight spectrometers

in single crystal and polycrystalline samples respectively shows them to be representative of a thermodynamic magnetic configuration. By analogy, the same is likely to be the case for the 3-**k** state realised in $USb_{0.85}Te_{0.15}$.

The further evidence furnished by neutron time-of-flight analysis (Figure 6c,d) shows that local, slow, long-time dynamics persist into the paramagnetic phase. This suggests that the scattering associated with the long-range magnetic order parameters may originate from local magnetic scattering units, which appear to characterise the multi-**k** magnetic configuration, supporting arguments previously advanced on the basis of the x-ray resonant scattering data [10]. In conjunction with this, the measured lower limit for the phase coherence time scale in the 3-**k** state imposes significant constraints on any theoretical interpretation.

6 Acknowledgements

EB, PJ and SBW would like to thank the European Commission for support in the frame of the 'Training and Mobility of Researchers' programme. This work was performed at the Institut Laue-Langevin, France, the European Synchrotron Radiation Facility, France, and the Swiss neutron spallation source SINQ, at the Paul Scherrer Institut, Switzerland; access to the Swiss neutron spallation source has been supported by the European Commission under the 6th Framework Programme through the Key Action: Strengthening the European Research Area, Research Infrastructures. Contract number: RII3-CT-2004-505925. Part of this work was made possible thanks to the support of the European Community-Access to Research Infrastructures action of the Improving Human Potential Programme in allowing access to the Actinide User Laboratory at the Institute for Transuranium Elements-Karlsruhe under Contract No. HPRICT-200100118.

Appendix A

The single crystal (mass 80 mg) of $UAs_{0.8}Se_{0.2}$ used in the neutron diffraction experiments and the $USb_{0.85}Te_{0.15}$ crystal were prepared at ETH Zurich, Switzerland. A second crystal of $UAs_{0.8}Se_{0.2}$ also used for x-ray resonant scattering was made twenty years later. The polycrystalline sample (34 g), prepared in two batches (denoted I and II) at the ITU, has been found to contain a small amount ($< 1\%$) of UO_2 impurity, as observed by comparing the relative time-of-flight integrated intensities of the UO_2 (111) and $UAs_{0.8}Se_{0.2}$ (111) peaks.

Within the estimated experimental error (± 1 K), T_N is the same in all samples of $UAs_{0.8}Se_{0.2}$. The heat capacity of the single crystal, used in the the neutron diffraction experiments, and Batch I, as used in the time-of-flight experiments, are shown in Figure 7. T^* is 51 K for the single crystal and 57 K for Batch I. Batch II displays similar behaviour, but T^* is 60 K. The microscopic origin of this sensitivity to sample preparation is unknown. It may be a further measure of the hysteretic nature of the discontinuous crystalline and magnetic transitions at this point. The M/H ratios, where M is the magnetisation and $H = 1000$ gauss is the magnetic field, of the single crystal and of Batch I are given in Figure 8.

$USb_{0.85}Te_{0.15}$ has the rocksalt structure. It becomes magnetically ordered at $T_N = 210$ K, entering an incommensurate phase and then, at $T_o \sim 160$ K, it enters a 3-**k** phase ($\mathbf{k} = \langle 0\ 0\ 1/2 \rangle$) that persists down to the lowest temperatures measured [13].

[Insert Figure 7 about here]

[Insert Figure 8 about here]

Figure Captions

Figure 1: Phase line for $UAs_{0.8}Se_{0.2}$ as a function of temperature. $\mathbf{k} = \langle 0\ 0\ 1/2 \rangle$.

Figure 2: A $\mathbf{k_3} = \tau + \langle kkk \rangle$ azimuth scan of $USb_{0.85}Te_{0.15}$ made by x-ray resonant diffraction on ID20 (ESRF). The scattering vector is (-1/2 -1/2 5/2) and the solid line is a model calculation based on a symmetry breaking vector which lies parallel to the [-1 -1 1] direction of the given reflection. Details of similar calculations are given in the appendix to Ref. [8].

Figure 3: Integrated intensity of $\langle 11k \rangle$ reflections of $UAs_{0.8}Se_{0.2}$ as a function of temperature, measured by neutron diffraction on D10 (ILL). The sample is the same as that used in the x-ray resonant scattering studies in Refs. [8-10].

Figure 4: Scans taken on D10 (ILL) along the [100] direction through $\mathbf{Q} =$ (3/2 -1/2 -1/2) at $T = 40$ K (left hand panel), $T = 65$ K (central panel) and $T = 130$ K (right hand panel). The line in the central panel is a Gaussian fit to the reflection profile; the width is similar to that observed in the $\mathbf{k_1}$ reflections. The $\lambda/2$ contamination is of the order of 1 to 2 counts on this scale.

Figure 5: Temperature dependences of the $\mathbf{k_1}$ (circles) and $\mathbf{k_3}$ (squares) integrated intensities as measured by neutron diffraction (closed points) and resonant x-ray scattering peak intensity [9] (open points). The data have been individually scaled to a common low temperature value.

Figure 6: Time-of-flight data from a polycrystalline ingot of $UAs_{0.8}Se_{0.2}$, measured on IN5 (ILL). Panels (a) and (b) show the integrated intensity (over an energy transfer range $-0.15 \leq \Delta E \leq 0.15$ meV) and energy linewidth of the elastic peak at the $\langle 1\ 1\ 1/2 \rangle$ position. Panels (c) and (d) give equivalent information for data averaged over the momentum transfer range $0.42 \leq Q \leq 1.41$ $Å^{-1}$, i.e. for scattering angles below the magnetic Bragg cut off value. The data in (c) have been adjusted for the integrated scattered solid angle to be comparable to (a).

Figure 7: The linear coefficient of the heat capacity of the 80 mg single crystal of $UAs_{0.8}Se_{0.2}$ (used in the present neutron diffraction studies and Refs. [8-10]), labelled 'original', and Batch I of the polycrystalline $UAs_{0.8}Se_{0.2}$ (used in the time-of-flight experiments on IN5, ILL and FOCUS, PSI), labelled 'new'. The insert shows data on an expanded scale around T^*, illustrating: (a) the amplitude hysteresis at the 2-**k** to 3-**k** transition, and (b) a marked sample dependency of T^*, which is not seen in the area under the anomaly (i.e. the change in entropy) or at T_N (see Figure 8).

Figure 8: The M/H ratio at $H = 1000$ gauss of the 80 mg single crystal (squares) and Batch I (circles) of $UAs_{0.8}Se_{0.2}$. Whilst the polycrystal has a higher dc susceptibility, T_N (defined by the point of maximum slope) is similar ($\pm$ 1 K) in both samples.

References

[1] see e.g. G.L. Squires, Introduction to the Theory of Thermal Neutron Scattering (Cambridge University Press, 1978).

[2] L.L. Hirst, Reviews of Modern Physics **69** 607 (1997); P.F. de Châtel and K. Ayuel, Physica B **266** 256 (1999).

[3] The non-trivial consequences of an arbitrary gauge leave the magnetisation with limited physical content.

[4] J.S. Kouvel and J. Kasper, Journal of Physics and Chemistry of Solids **24** 529 (1963).

[5] Some authors use a non-orthogonal basis set.

[6] M. Kuznietz, P. Burlet, J. Rossat-Mignod and O. Vogt, Journal of Magnetism and Magnetic Materials **69** 12 (1987).

[7] M.J. Longfield, W.G. Stirling, E. Lidström, D. Mannix, G.H. Lander, A. Stunault, G.J. McIntyre, K. Mattenberger and O. Vogt, Physical Review B **63** 134401 (2001).

[8] M.J. Longfield, J.A. Paixao, N. Bernhoeft and G.H. Lander, Physical Review B **66** 054417 (2002).

[9] N. Bernhoeft, J.A. Paixao, C. Detlefs, S.B. Wilkins, P. Javorsky, E. Blackburn and G.H. Lander, Physical Review B **69** 174415 (2004).

[10] G.H. Lander and N. Bernhoeft, Physica B **34** 345 (2004).

[11] M. Loewenhaupt, G.H. Lander, A. Murani and A. Murasik, Journal of Physics C **15** 6199 (1982).

[12] P. Giudicelli, B. Roessli, A. Stunault, J. Ollivier, A. Amato, H. Sugawara and N. Bernhoeft, Journal of Magnetism and Magnetic Materials **272-276** E141 (2004); P. Giudicelli and N. Bernhoeft, Europhysics Letters **67** 117 (2004).

[13] P. Burlet, S. Quezel, J. Rossat-Mignod, O. Vogt and G.H. Lander, Physica B **102** 271 (1980).

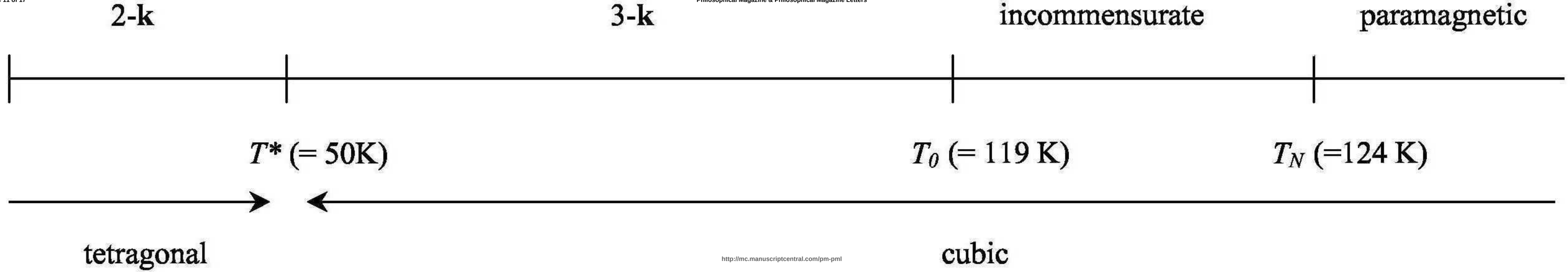
2-k
3-k
incommensurate
paramagnetic
T* (= 50K)
T0 (= 119 K)
TN (=124 K)
tetragonal
cubic

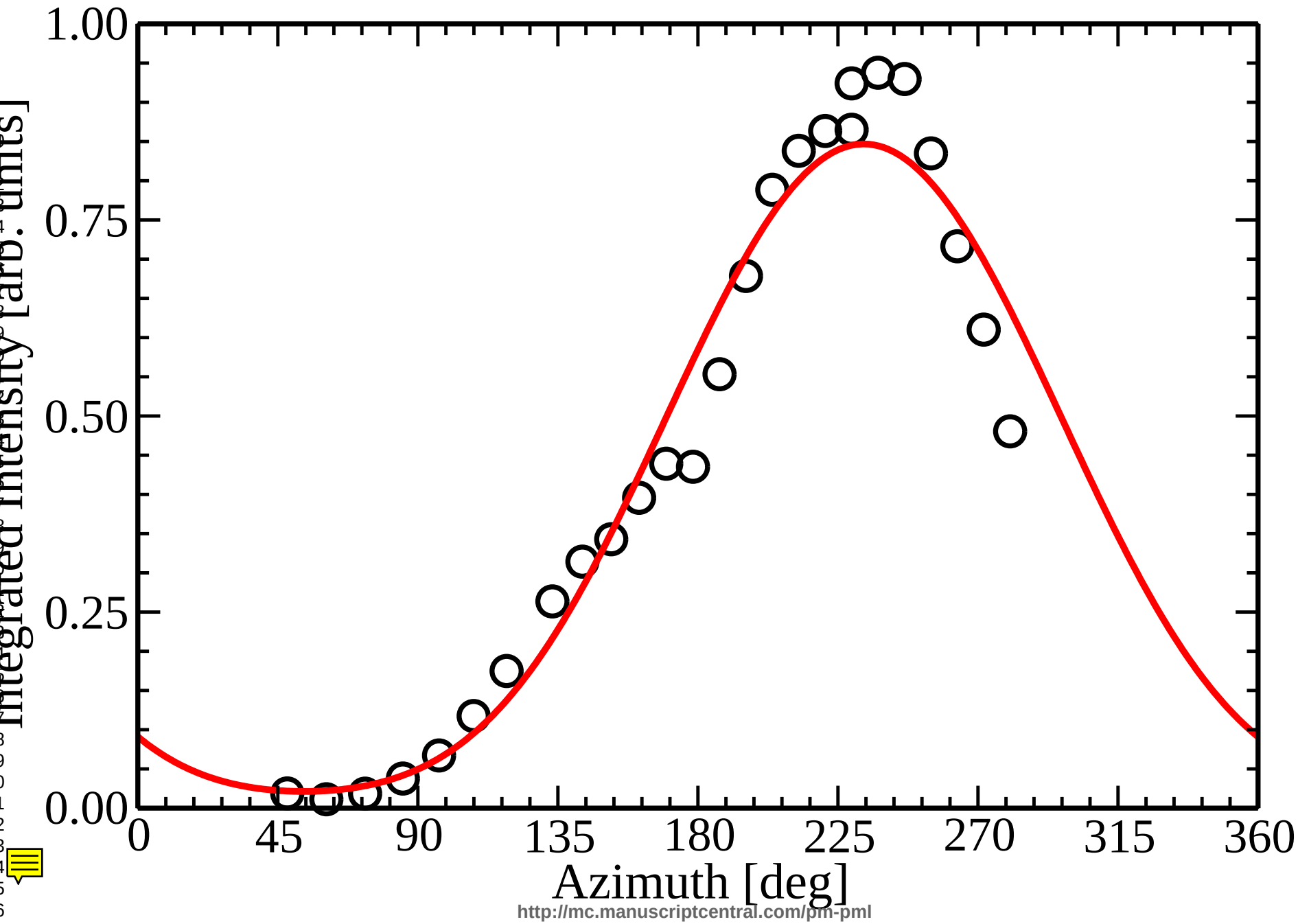
1.00
0.75
0.50
0.25
0.00
Integrated Intensity [arb. units]
0
45
90
135
180
225
270
315
360
Azimuth [deg]

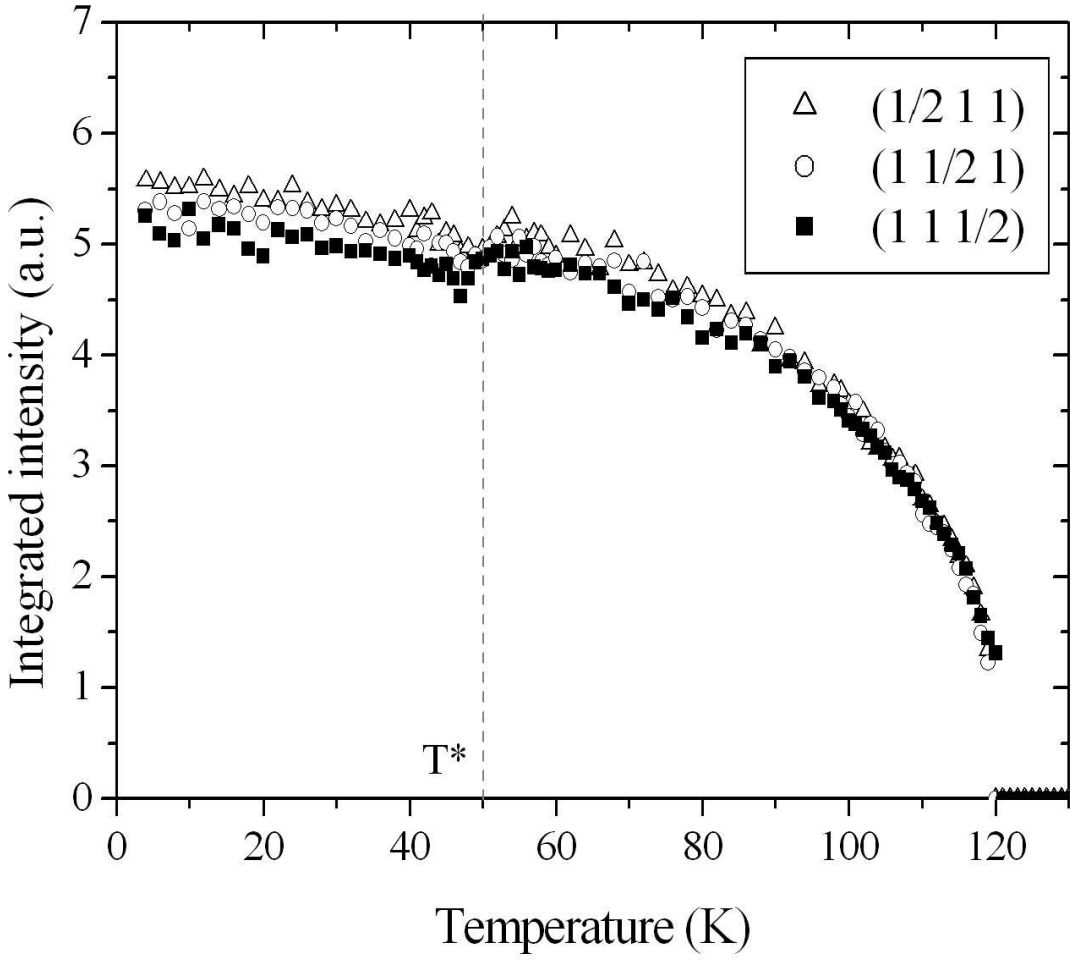
Integrated intensity (a.u.)
Temperature (K)
T*
(1/2 1 1)
(1 1/2 1)
(1 1 1/2)
0
1
2
3
4
5
6
7
0
20
40
60
80
100
120

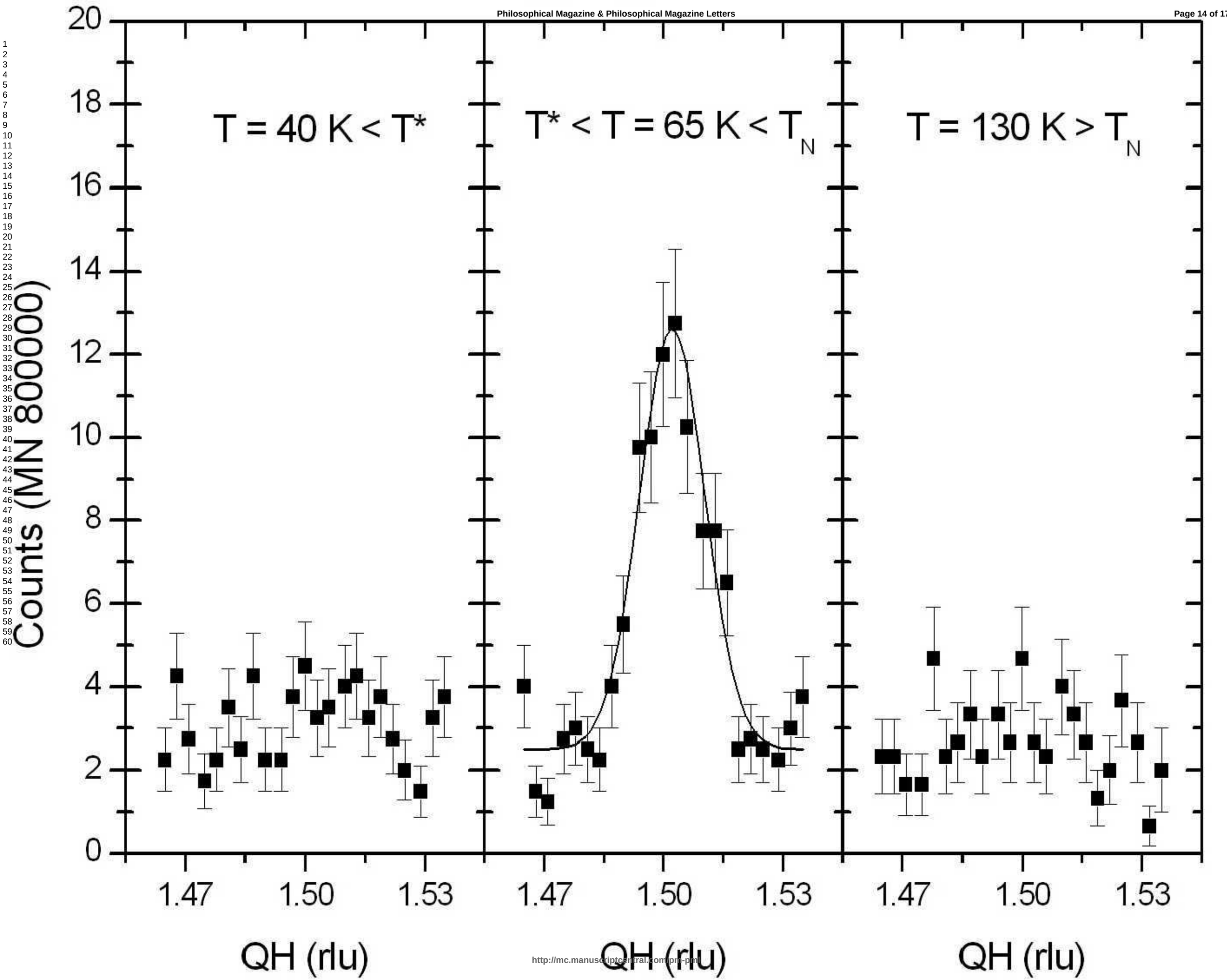
T = 40 K < T*
T* < T = 65 K < T_N
T = 130 K > T_N
Counts (MN 800000)
20
18
16
14
12
10
8
6
4
2
0
1.47
1.50
1.53
QH (rlu)

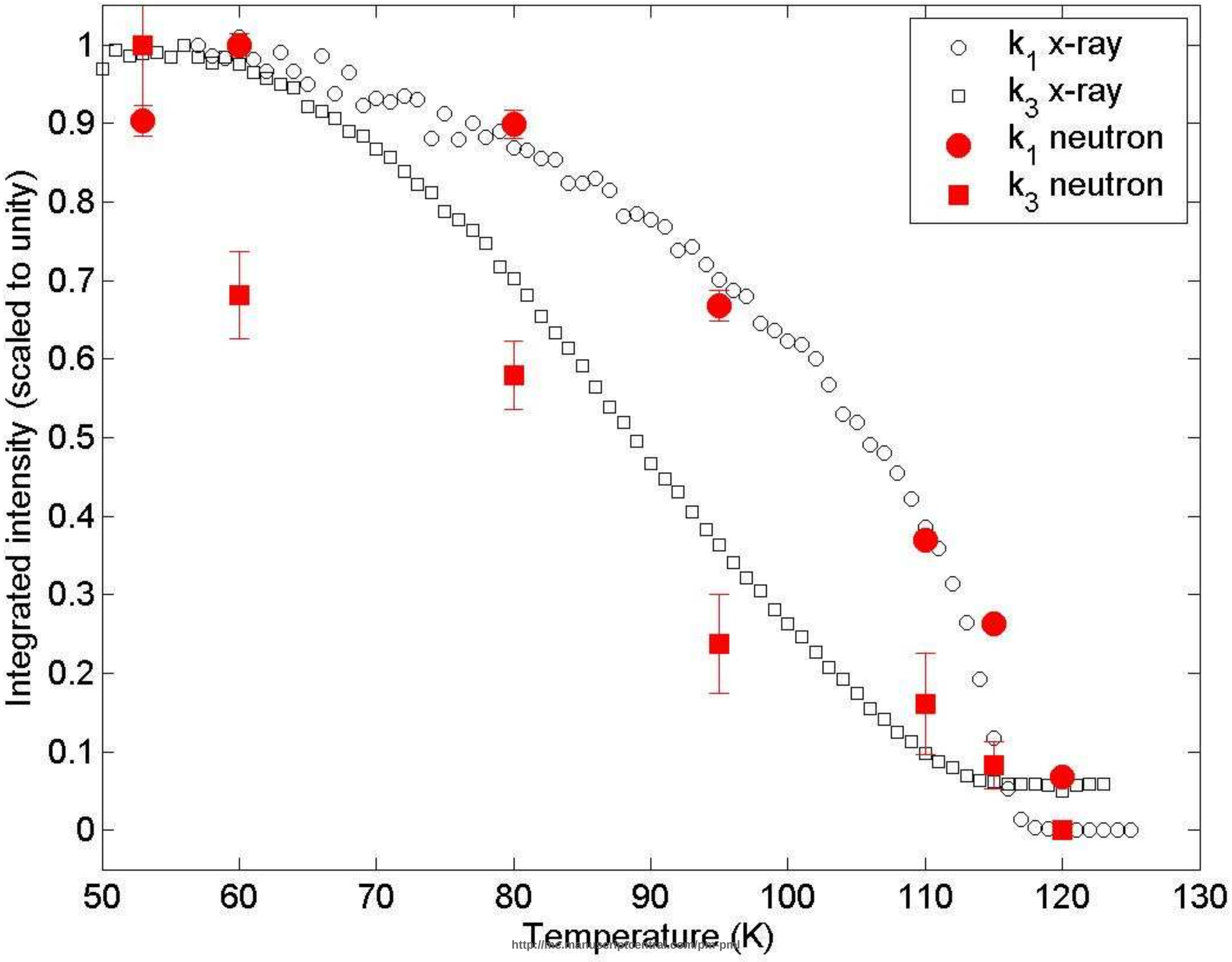

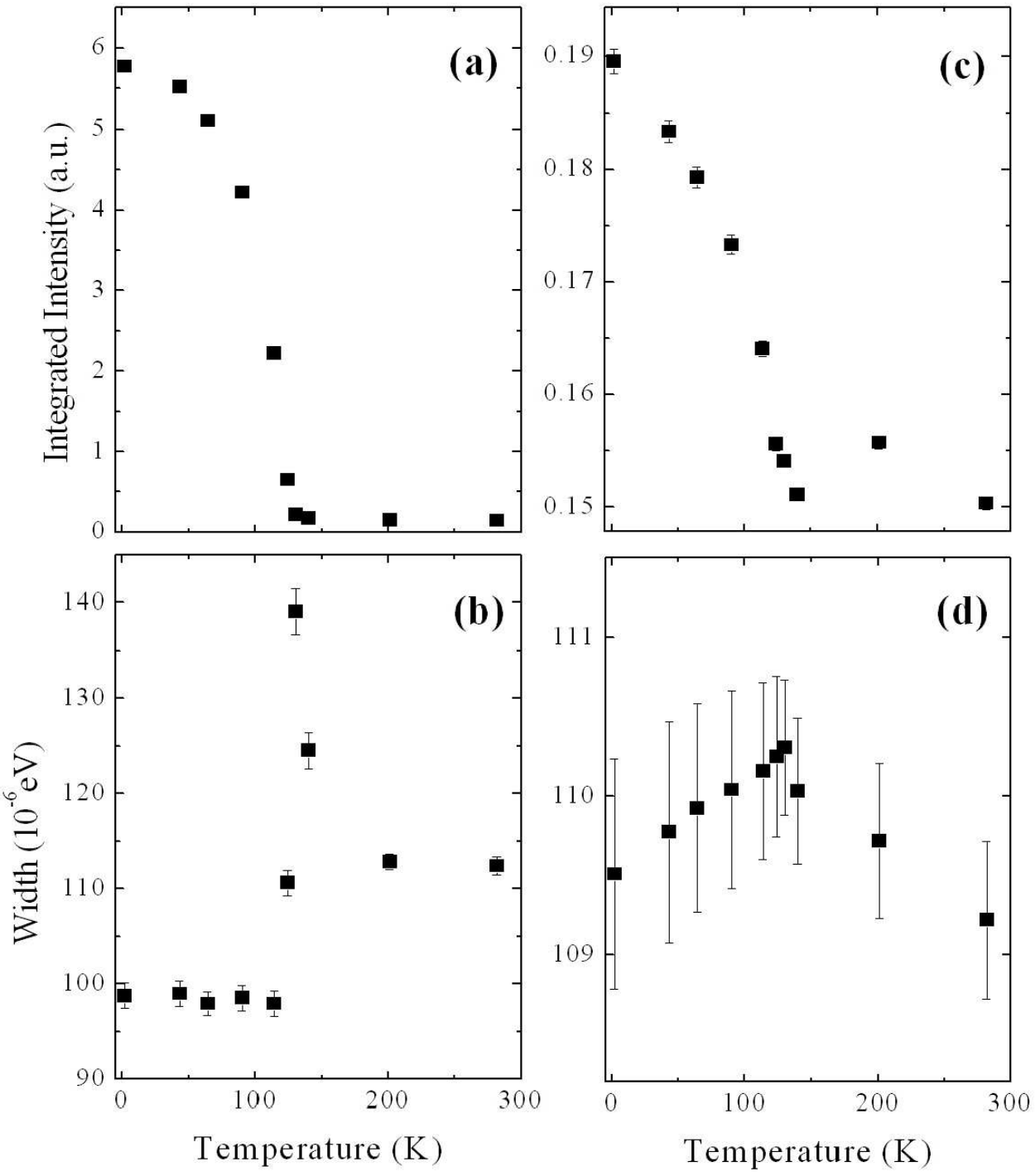
(a)
(b)
(c)
(d)
Integrated Intensity (a.u.)
Width (10^{-6} eV)
Temperature (K)
Temperature (K)

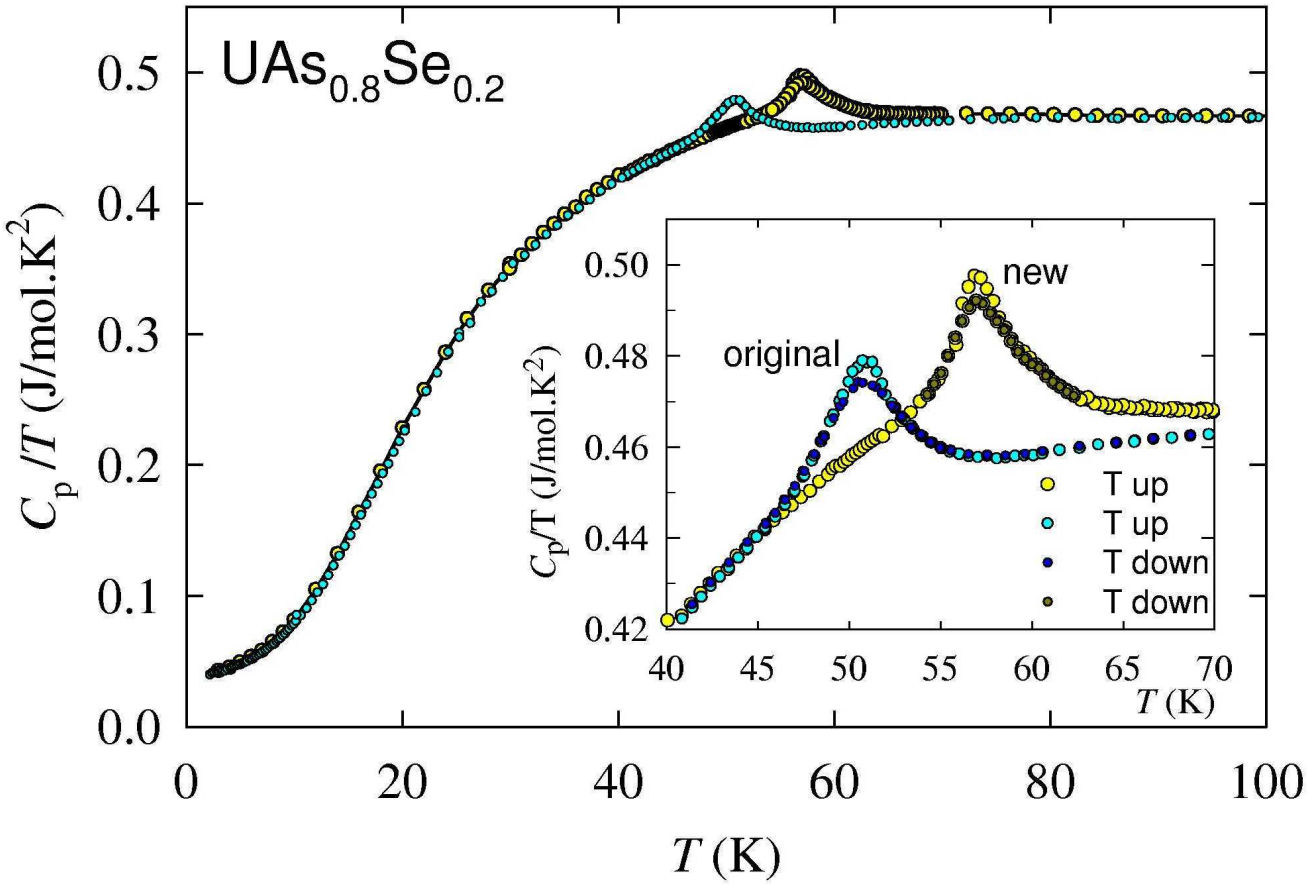
UAs0.8Se0.2
Cp /T (J/mol.K2)
T (K)
0.0
0.1
0.2
0.3
0.4
0.5
0
20
40
60
80
100
Cp/T (J/mol.K2)
0.42
0.44
0.46
0.48
0.50
40
45
50
55
60
65
70
T (K)
original
new
T up
T up
T down
T down

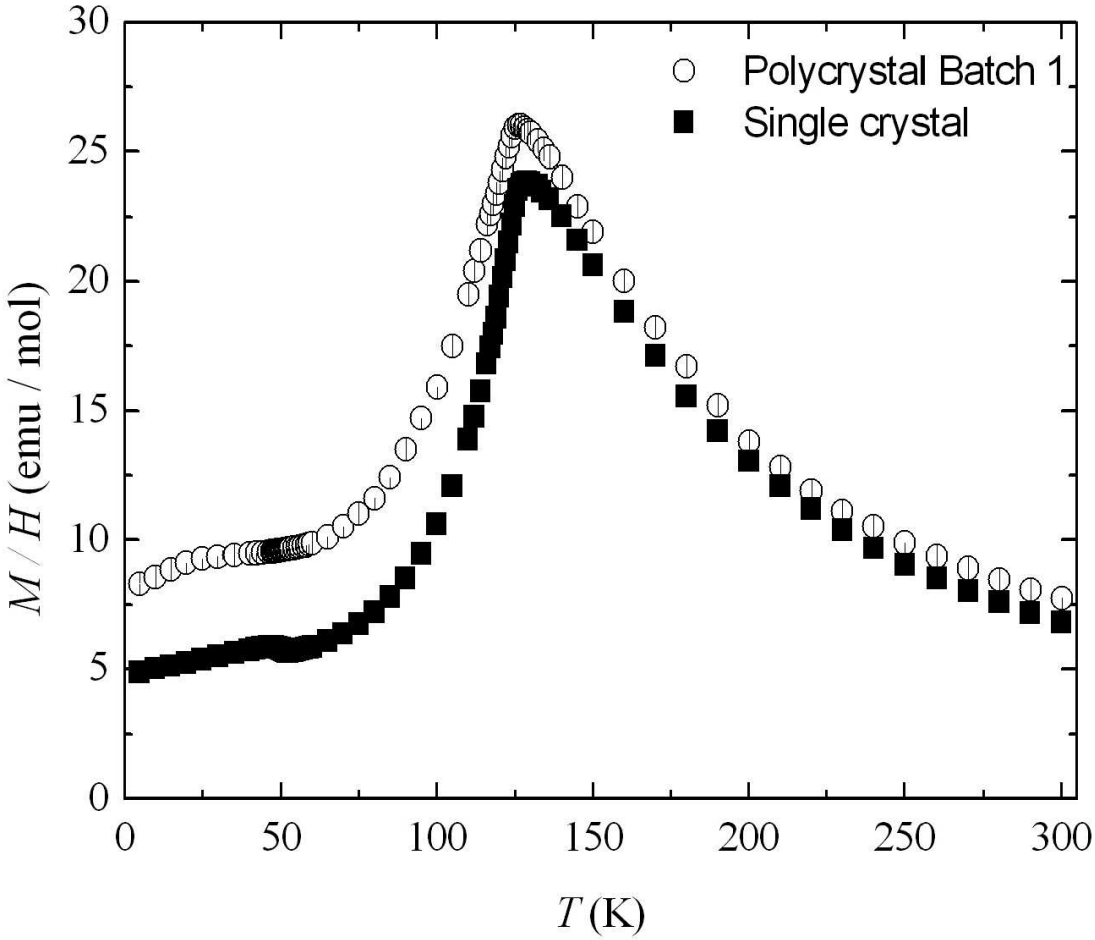
Polycrystal Batch 1
Single crystal
M / H (emu / mol)
T (K)
0
5
10
15
20
25
30
0
50
100
150
200
250
300